
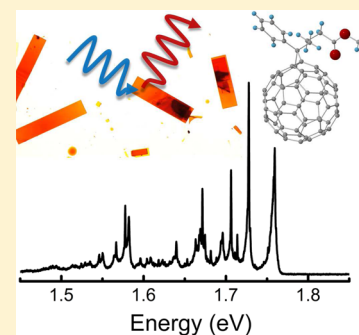


# Low-Temperature Photoluminescence Spectroscopy of Solvent-Free PCBM Single-Crystals

Giulia Tregnago,<sup>†,||</sup> Michael Wykes,<sup>‡,||</sup> Giuseppe M. Paternò,<sup>†</sup> David Beljonne,<sup>§</sup> and Franco Cacialli<sup>\*,†</sup><sup>†</sup>Department of Physics and Astronomy and London Centre for Nanotechnology, University College London, Gower Street, London, WC1E 6BT, United Kingdom<sup>‡</sup>Madrid Institute for Advanced Studies, IMDEA Nanoscience, C/Faraday 9, Campus Cantoblanco, 28049 Madrid, Spain<sup>§</sup>Laboratory for Chemistry of Novel Materials, Université de Mons, 20, Place du Parc, 7000 Mons, Belgium Supporting Information

**ABSTRACT:** PCBM ([6,6]-phenyl-C<sub>61</sub>-butyric acid methyl ester) is a highly soluble C<sub>60</sub> derivative that is extensively used in organic solar cells, enabling power conversion efficiencies above 10%. Here we report, for the first time to the best of our knowledge, the photoluminescence of high-quality solvent-free PCBM crystals between room temperature and 4 K. Interestingly, the PL spectra of these crystals become increasingly structured as the temperature is lowered, with extremely well-resolved emission lines (and a minimum line width of ~1.3 meV at 1.73 eV). We are able to account for such a structured emission by means of a vibronic coupling model including Franck–Condon, Jahn–Teller and Herzberg–Teller effects. Although optical transitions are not formally forbidden from the low-lying excited states of PCBM, the high symmetry of the electronically active fullerene core limits the intensity of the 0–0 transition, such that Herzberg–Teller transitions which borrow intensity from higher-lying states represent a large part of the observed spectrum. Our simulations suggest that the emissive state of PCBM can be considered as a mixture of the T<sub>1g</sub> and H<sub>g</sub> excited states of C<sub>60</sub> and hence that the H<sub>g</sub> state plays a larger role in the relaxed excited state of PCBM than in that of C<sub>60</sub>.



## INTRODUCTION

PCBM ([6,6]-Phenyl C<sub>61</sub> butyric acid methyl ester) is currently the most important C<sub>60</sub> derivative,<sup>1,2</sup> owing to the efficiency of charge transfer from nearby photoexcited molecular states, which makes it the elective electron acceptor in highly efficient bulk heterojunction (BHJ) solar cells, and to other advantages, such as lower synthetic costs compared to C<sub>70</sub> derivatives. In spite of their relevance to organic optoelectronics, little attention has been dedicated to PCBM's luminescent properties,<sup>3,4</sup> although they may provide crucial insight into the fundamental energetics of this material, especially in its crystalline phase. Furthermore, a recent study by Lanzani et al.<sup>5</sup> found that the primary process upon photoexcitation is ultrafast energy transfer from poly(3-hexylthiophene-2,5-diyl) (P3HT) to PCBM, thus challenging the accepted view of the dominance of ultrafast electron transfer at the polymer/PCBM interface, and suggesting that an improved understanding of the low-lying excited states of PCBM should be a prerequisite for exploiting approaches to engineer the energy transfer process and increase device efficiencies. Both the molecular packing and the details of the nanostructure of fullerene-based BHJs have been shown recently to have a crucial impact on the device efficiency.<sup>6</sup> OPV devices based on P3HT and PCBM blends show better performance upon formation of aggregate phases in either components following thermal annealing.<sup>7</sup> In particular, PCBM aggregates have been proven to assist ultrafast long-range charge separation.<sup>8,9</sup> However, the crystal structure of PCBM turns out to be strongly dependent on the

solvent from which the crystals are grown and that is present in the crystals themselves as an inclusion.<sup>10</sup> Only recently, solvent-free PCBM single-crystals were reported with a monoclinic structure following solvent extraction in vacuum<sup>11</sup> or via a thermal treatment,<sup>12</sup> thereby allowing fundamental structure–property investigations without the solvent dependence.<sup>13</sup> In particular, crystallite geometries are fundamental to investigate the electronic states involved in charge separation.<sup>14</sup>

Here, we report a combined spectroscopic and computational investigation of the photoluminescence (PL) of PCBM in the amorphous, polycrystalline, and crystalline phase. The evolution of the emission for the single-crystal discloses a progressively better-resolved structure as the temperature is lowered down to 4 K. We are able to describe such an evolution quantitatively by using a combined approach in which Jahn–Teller (JT) and Franck–Condon (FC) progressions are built upon Herzberg–Teller (HT) intensity-borrowing transitions.

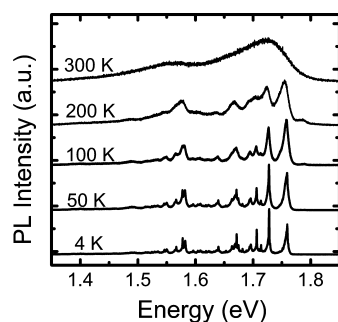
## RESULTS

In Figure 1 we report the fluorescence spectra of PCBM single-crystals as a function of temperature in the 4–300 K range. As the temperature is decreased, the PL emission undergoes a striking evolution with many more (well-resolved) transition lines than expected from the room temperature spectra. An

Received: March 10, 2015

Revised: April 29, 2015

Published: May 15, 2015

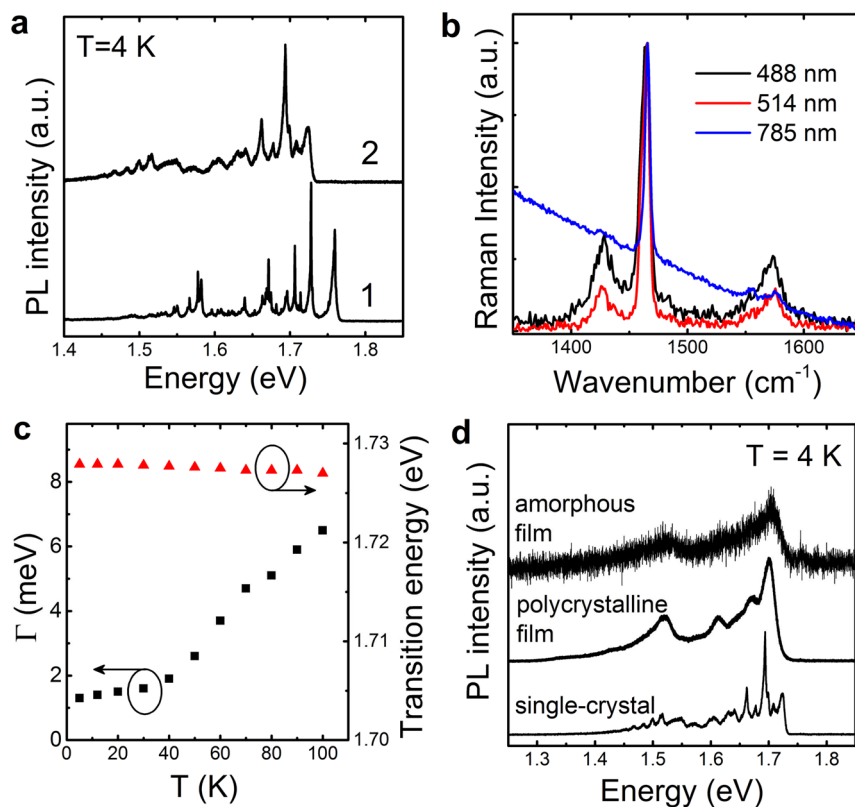


**Figure 1.** Photoluminescence as a function of temperature (in the range 4–300 K) for a PCBM single-crystal. Spectra have been normalized with respect to their maximum intensity. Excitation is through an optical microscope (2  $\mu\text{m}$  diameter) and with a He–Ne laser (632.8 nm).

apparent blue-shift is observable, first of all, by comparing the 200 K spectrum (with most intense peak at 1.76 eV) to the 300 K one (peaking at 1.73 eV). Rather than a blue-shift of the emission, this could actually be due to a relative intensity redistribution between the various (inhomogeneously broadened) lines when lowering the temperature. However, it is then somewhat surprising that we only observe a minor temperature dependence of the relative intensities for  $T < 200$  K. Even though the very weak peak at 1.79 eV eventually disappears at the lowest temperatures, the more intense peaks only show very

minor variability: for example, the relative intensity of the peaks at 1.76 and 1.58 eV is comparable, as also is the case for the peaks at 1.73 and 1.67 eV. However, a blue-shift upon cooling is rather unusual for conjugated (macro)molecules,<sup>15</sup> whose emission notoriously red-shifts upon cooling, owing to their planarization induced by the freezing of the vibrational modes. A blue-shift is therefore unexpected, although we consider that the spherical structure of PCBM (and  $\text{C}_{60}$ ) and the concomitant complex interplay of state-mixing within the context of FC, JT, and HT effects (which we further discuss in detail below) might alter significantly the evolution of the excited states with respect to “linear” ribbon-like organic semiconductors. Other effects, namely spectral diffusion to trap states, might also be present at the highest temperature, and be (at least partially) suppressed upon cooling, thereby justifying the apparent blue-shift.

In fact, while most PCBM crystals emit low-temperature spectra as reported in Figure 1, in some cases we observed spectrally red-shifted, and less well-resolved emission, although still highly structured and with a similar temperature dependence. We report an example in Supporting Information (SI) Figure S1, and compare the 4 K spectra of the crystals of Figure 1 and S1 in Figure 2a. Here we note a rigid shift in energy of about 35 meV of the spectra with respect to one another. Nevertheless, the distribution of the vibrational peaks is similar, suggesting that emission occurs from similar types of excited states with different origins. We also observe small differences



**Figure 2.** (a) Normalized low-temperature fluorescence of two different single crystals: the rigid shift of about 35 meV of spectrum 2 with respect to spectrum 1 is related to the presence of a trap. (b) Normalized Raman spectra of PCBM single-crystals at different wavelengths (laser power at the sample surface of  $\sim 0.1$  mW) at room temperature. The strongest peak (pentagonal-pinch mode  $A_g(2)$  of  $\text{C}_{60}$ ) is at 1464  $\text{cm}^{-1}$  for the 488 nm curve (black) and 1465  $\text{cm}^{-1}$  for the 514 and 785 nm curves (red and blue respectively). (c) Energy of the second well-resolved transition (at about 1.73 eV) for spectrum 1 in (a) and the temperature dependence of the line width. Above 100 K the broadening of the peaks prevents an accurate quantification of the line width. (d) Low-temperature fluorescence of PCBM as amorphous film, polycrystalline film and single-crystal. Note the trend toward a progressively better resolved PL with increasing crystallinity of the samples.

in relative peak intensities between the two spectra. There are many potential explanations both for the red-shift and for the additional subtle changes. For example, these could be due to a morphological crystal defect red-shifting the 0–0 transition via solvatochromic effects, thus influencing state-mixing and hence spectral shape (see below).

The presence of chemically degraded PCBM could also provide a potential alternative interpretation. It is well-known that fullerenes can dimerize in the solid state upon exposure to ultraviolet (UV) and visible light;<sup>16</sup> however, we can rule out this possibility by means of the Raman spectra reported in Figure 2b. Here, we see that the pentagonal pinch mode  $A_g(2)$  for the  $C_{60}$  cage peaks at  $1464\text{ cm}^{-1}$  as reported for pristine (nondimerized) PCBM.<sup>17</sup> Therefore, we assign the red-shifted spectrum to an emission from a deep trap. Indeed, similar behavior has been reported in  $C_{60}$  single-crystals<sup>18</sup> with traps that were found to be red-shifted by 100 meV relative to bulk  $C_{60}$ .

Interestingly, however, the 300 K spectrum of SI Figure S1, is also red-shifted compared to the  $T \leq 200\text{ K}$ , thereby suggesting that the apparent blue-shift of the spectra upon cooling from 300 to 200 K is not to be assigned to spectral diffusion, but rather to solvatochromism or a different interplay of HT, JT, and FC effects.

The PL spectrum at 4 K shows very well-resolved emission lines with a minimum fwhm (full width half maximum) of 1.3 meV. Such a narrow spectral line width demonstrates the high-quality of the single-crystals. In Figure 2c, we report the temperature evolution (in the range 5 to 100 K) of both line width and spectral position of the peak at 1.73 eV. Interestingly, while there is only a marginal spectral shift of this peak ( $<0.5\text{ meV}$ ), the line width is temperature-dependent. The line width is nearly constant for  $T < 40\text{ K}$ , but increases more prominently and nearly linearly with increasing temperature, for  $T > 40\text{ K}$ . We suggest that such a strong temperature dependence is due to a mostly homogeneous (dynamic) mechanism, associated with changes in the thermal distributions of molecular vibrations and crystal phonon modes.

To obtain further insights into the effect of structural disorder on the PL spectra, we also consider the low-temperature PL spectra of the crystals (Figure 2d) and of amorphous and polycrystalline films (powder XRD data in SI Figure S2) and compare them with those at room temperature (SI Figure S3). As expected, we observe only minor differences between the low-temperature (4 K) and room temperature PL spectra of the amorphous film. In particular, only a minor sharpening of the emission peaks is noted when lowering the temperature. The polycrystalline film shows an increased number of better-resolved peaks at 4 K, compared to the room temperature spectrum, and with respect to the amorphous film, even though a relatively broad band is still visible. We also note that the peak structure only starts to appear below 50 K.

We emphasize that, even if less structured than the single-crystal spectrum, the 4 K spectra of amorphous and polycrystalline samples also feature a progressive, albeit moderate, sharpening of the line widths. This can be interpreted in the sense that the structural inhomogeneity, although clearly present, does not translate into such a preponderant (static) energetic disorder in PCBM to prevent the observation of any line width reduction. Although a direct comparison between neutral excitations and charge carriers should be considered with caution, this is in line with the

widely accepted view that charge transport in fullerenes is rather tolerant to positional disorder (also partly explained by the large nearest neighbor coordination number).<sup>11</sup>

Interestingly, amorphous, polycrystalline and single-crystal samples of  $C_{60}$  fullerene<sup>19,20</sup> are characterized by a similar trend, despite the lower symmetry of PCBM compared to  $C_{60}$ . Sassara et al. reported a thorough study of the electronic states and transitions for  $C_{60}$  including assignments of vibronic transitions based on a comparison of simulated and experimental spectra measured in inert Ar and Ne matrices at 4 K.<sup>21</sup> Transitions from the three lowest quasi-degenerate excited states (of  $T_{1g}$ ,  $T_{2g}$  and  $G_g$  symmetry) to the ground state ( $A_g$ ) are symmetry forbidden. Thus, emission from such states occurs through vibronic coupling with a higher electronic state of *ungerade*-symmetry via a mechanism known as HT intensity borrowing. Radiative transitions to the ground state arise from the vibronically induced HT false origins of each HT-coupled vibration, each convoluted with its own FC progression. Furthermore, the  $T_{1g}$ ,  $T_{2g}$  and  $G_g$  states have degenerate components that undergo a JT geometrical distortion that removes the degeneracy and thus lowers the symmetry. Transitions arising from vibronic coupling to nontotally symmetric JT modes are seen in the low temperature spectra of  $C_{60}$ .<sup>21</sup> The selection rules for the transitions are determined by the high  $I_h$  symmetry of  $C_{60}$ . Upon derivatization of  $C_{60}$  to form PCBM the symmetry is lowered due to the side chain. However, despite the lower molecular symmetry, we note many similarities between the low-temperature PL spectra of PCBM and  $C_{60}$  single crystals. In light of these similarities, we extend Sassara et al.'s simulations of  $C_{60}$  PL to PCBM.

In Sassara et al.'s study the simulated vibronic envelopes of  $T_{1g}$ ,  $T_{2g}$  and  $G_g$  states were constructed from HT, FC, and JT couplings obtained from quantum-chemical (QC) calculations, and the total PL was modeled by combining the vibronic envelopes of each state with weights (i.e., state-mixing coefficients) obtained empirically to provide the best match to the experimentally observed spectra.<sup>21</sup> Regrettably, the modeling approach applied to  $C_{60}$ , namely calculating the vibronic envelopes of each diabatic excited state ( $T_{1g}$ ,  $T_{2g}$ ,  $G_g$ , i.e., the symmetry-pure, unmixed states of the system), cannot be readily applied to PCBM. This is because, in PCBM, the lower symmetry imposes a mixing of states, preventing the study of the underlying higher-symmetry diabatic states. The multiply degenerate states of  $C_{60}$  are replaced with 10 quasi-degenerate states of mixed character in PCBM. This also presents two additional hurdles to QC simulation of vibronic coupling in the absence of symmetry; the first one relates to describing correctly the relative energies of the 10 quasi-degenerate states and hence their propensity to mix with each other, and the second is due to the difficulties in obtaining relaxed excited state geometries (e.g., root-flipping).<sup>22</sup> Indeed, relaxing symmetry constraints and thus allowing for state-mixing results in simulated vibronic structure of  $C_{60}$  and PCBM which differs wildly from the observed PL of each system (see SI Figures S4 and S5). This confirms that correctly describing the state mixing in  $C_{60}$  (and hence related fullerenes) is indeed too great a challenge for the TD-DFT-based method used and that this approach should not be adopted for reliable simulation of PCBM PL spectra.

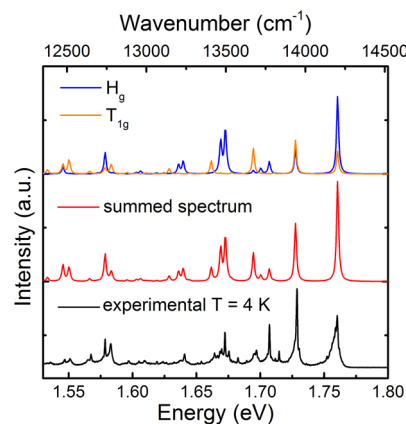
Given the similarities between  $C_{60}$  and PCBM PL and the success of Sassara et al.'s empirically tuned QC-based approach applied to  $C_{60}$ , here we develop a model of PCBM PL based on

Sassara et al.'s diabatic-state model of  $C_{60}$ , making some empirical adjustments of our own to account for the observed differences between PCBM and  $C_{60}$  spectra. The retuning of Sassara et al.'s  $C_{60}$  model to interpret PCMB PL is justified if one considers the pendant group in PCBM as a perturbation to the  $C_{60}$  electronic structure. QC calculations support this hypothesis, showing that the electron density for the HOMO/LUMO of the PCBM is mostly located on the  $C_{60}$  core with only little density residing on the side chain.<sup>23,24</sup> The need for adaptations of Sassara et al.'s models can be readily appreciated by plotting the  $C_{60}$  PL in Ar and Ne matrices and the single-crystal PCBM PL on the same axes (SI Figure S6). Adjustments are required to take into account the sensitivity of state-mixing (and hence PL vibronic structure) to the PCBM single-crystal environment and the chemical substitutions in PCBM. Sassara et al.'s model<sup>21</sup> of  $C_{60}$  PL was thus hand-tuned in several incremental steps to develop our model of PCBM PL. First, the electronic origin was set to  $14200\text{ cm}^{-1}$  ( $1.76\text{ eV}$ ) to coincide with the first peak in PCBM PL (SI Figure S7). This is close to the value of  $14629\text{ cm}^{-1}$  observed in  $C_{60}$  single-crystals<sup>25</sup> yet significantly red-shifted relative to the electronic origins of  $C_{60}$  in Ar and Ne matrices at  $15487$  and  $15627\text{ cm}^{-1}$ , respectively.<sup>21</sup> Following this, the impact of variation in the weights of the  $T_{1g}$ ,  $T_{2g}$ , and  $G_g$  states was explored (in a similar way that Sassara et al. varied state weights to reproduce  $C_{60}$  spectra in different media). A plot of the individual state components suggests that the  $G_g$  state is responsible for the band around  $13500\text{ cm}^{-1}$  (SI Figure S8).  $T_{1g}$ ,  $T_{2g}$ , and  $G_g$  weights of 40%, 20%, and 30%, respectively provided the best overall agreement with the PCBM spectra.

However, the intense 0–0 transition, not strictly symmetry-forbidden in PCBM, is clearly missing from the model shown in SI Figure S8, as are peaks likely to be FC/JT progressions built upon it. An electronic origin  $\sim 2.5$  times more intense than the most intense HT origin was thus added to the vibronic envelope of each state with FC and JT progressions built on top. The FC/JT progressions reproduce the previously missing peak at  $13940\text{ cm}^{-1}$  ( $1.73\text{ eV}$ ), see SI Figure S9, although the intensity of this new peak relative to the 0–0 is underestimated. Assuming the  $13940\text{ cm}^{-1}$  peak observed experimentally is indeed an FC/JT replica of the 0–0 suggests that the Huang–Rhys factor for the mode concerned ( $1\text{ h}_g$ ) is underestimated. In fact, it was suggested by Sassara et al. that one of the calculated JT vibronic couplings in the model (between the  $T_{1g}$  state and  $1\text{ h}_g$  vibration) was likely underestimated due to limitations of the QC method used.<sup>21</sup> Sassara et al. hence adjusted the value of this parameter to improve agreement with the  $C_{60}$  spectra in Ar and Ne, but did not report the adjusted value (only reporting the calculated value likely to be underestimated).<sup>25</sup> In a similar approach to that adopted by Sassara et al., we empirically adjust the same Huang–Rhys factor that Sassara et al. tuned (between the  $T_{1g}$  state and  $1\text{ h}_g$  vibration) from 0.06 to 1.5. This improves the relative intensities of the 0–0 and  $13940\text{ cm}^{-1}$  peaks (SI Figure S10). It is possible that the increase from 0.06 to 1.5 is larger than the change Sassara et al. made, however, such a change may be justified by the structural differences between  $C_{60}$  and PCBM.

Although the simulated spectrum shown in SI Figure S10 reproduced many of the features of the experimental PCBM spectrum, the third most intense peak, at  $13770\text{ cm}^{-1}$  ( $1.71\text{ eV}$ ), was missing. It was then noted that none of the peaks of the  $T_{1g}$ ,  $T_{2g}$ , and  $G_g$  vibronic envelopes (placed on an origin of

$14200\text{ cm}^{-1}$ ) had a peak at  $13770\text{ cm}^{-1}$ . However, the vibronic envelope of the  $H_g$  state, for which the vibronic coupling parameters are also listed by Sassara et al., did feature a transition with non-negligible intensity at that energy once placed at an origin of  $14200\text{ cm}^{-1}$ . Furthermore, it was noted that the vibronic envelope of the  $H_g$  state was quite similar to that of the  $G_g$  state and could also account for the band in the PCBM spectrum at  $13500\text{ cm}^{-1}$  not present in either the  $T_{1g}$  or  $T_{2g}$  vibronic envelopes (see SI Figure S11). The  $H_g$  state did not form part of Sassara et al.'s model of  $C_{60}$  PL as QC calculations placed it slightly higher in energy than the quasi-degenerate  $T_{1g}$ ,  $T_{2g}$ , and  $G_g$  states and the experimental spectra were well reproduced without including it. However, the mixing of states has been shown to be highly dependent on the environment. This is likely because the solvatochromic shift upon changing environment is state-dependent and the mixing of states depends on their relative energies. The fact that vibronic peaks of the  $H_g$  state can reproduce otherwise missing features suggests that the  $H_g$  state is lower in energy in PCBM crystals than in  $C_{60}$  experiences (perhaps due to a greater solvatochromic stabilization and/or difference in chemical structure) and is hence mixed into the emissive state in PCMB crystals. A final modification to the simulated spectrum was therefore made, changing the state mixing to 50%  $T_{1g}$ , 50%  $H_g$ , resulting in the spectrum shown in Figure 3. This



**Figure 3.** Convolved spectra based on Herzberg–Teller, Franck–Condon, and Jahn–Teller computed transition lines for the  $H_g$  (blue) and  $T_{1g}$  (yellow) states. The summed spectrum (red) results from a linear combination of 0.5  $H_g$  and 0.5  $T_{1g}$  and is compared with the experimental data (black).

reproduces well the experimental PCBM single-crystal data (also plotted in Figure 3), though there are some minor but non-negligible discrepancies. These include the relative intensities of the first and second peak (for decreasing energies), the relative energies and intensities of the three features at  $\sim 1.70\text{ eV}$ , and the relative intensities of the two features near  $1.58\text{ eV}$ . We attribute such slight discrepancies to our assumption that PCBM fluorescence can be simulated using a model developed for  $C_{60}$ . The chemical differences between  $C_{60}$  and PCBM might indeed shift some of the vibrational frequencies in PCBM, an effect we have not taken into account here. As such, the challenging problem of computing the vibrational spectra of PCBM from quantum-chemical calculations could yet be a valuable contribution to understanding PCBM PL and should be revisited in future studies.

## CONCLUSIONS

Here we report, for the first time to the best of our knowledge, the photoluminescence of high-quality solvent-free PCBM crystals between room temperature and 4 K. Interestingly, the PL spectra of these crystals become increasingly structured as the temperature is lowered, with extremely well-resolved emission lines (and a minimum line width of  $\sim 1.3$  meV at 1.73 eV). We are able to account for such a structured emission by means of a vibronic coupling model including FC, JT and HT effects. We build upon the approach of Sassara et al., who interpreted the fine structure of  $C_{60}$  fluorescence by combining vibronic coupling parameters derived from quantum chemical calculations with an empirical tuning of some of the vibronic coupling parameters and the participation of the various low-lying excited states in the emissive state. Specifically, Sassara et al.'s model of  $C_{60}$  PL was hand-tuned in several incremental steps to develop our model of PCBM PL. Though optical transitions are not formally forbidden from the low-lying excited states of PCBM, the high symmetry of the electronically active fullerene core limits the intensity of the 0–0 transition, such that HT transitions which borrow intensity from higher-lying states represent a large part of the observed spectrum. Our simulations suggest that the emissive state of PCBM can be considered as a mixture of the  $T_{1g}$  and  $H_g$  excited states of  $C_{60}$  and hence that the  $H_g$  state plays a larger role in the relaxed excited state of PCBM than in that of  $C_{60}$ .

## ASSOCIATED CONTENT

### Supporting Information

Experimental details. Fluorescence spectra as a function of temperature and X-ray diffraction patterns for amorphous and polycrystalline PCBM. Additional details concerning the simulated spectra. The Supporting Information is available free of charge on the ACS Publications website at DOI: 10.1021/acs.jpcc.5b02345.

## AUTHOR INFORMATION

### Corresponding Author

\*Tel: +44 20-7679-4467; e-mail: f.cacialli@ucl.ac.uk.

### Author Contributions

<sup>||</sup>These authors contributed equally to this work.

### Notes

The authors declare no competing financial interest.

## ACKNOWLEDGMENTS

We are grateful to Dr. Christoph Salzmann, Jacob Shephard, and Dr. Guy Matmon for their help with the low-temperature fluorescence measurement setup. We thank the EC Seventh Framework Programme (FP7/2007-2013) under Grant Agreement No. 264694 (GENIUS), the EU Horizon 2020 Research and Innovation Programme under Grant Agreement N. 643238 (SYNCHRONICS), as well as the Royal Society and the EPSRC. M.W. thanks the European Commission for his Marie Curie Fellowship (FP7-PEOPLE-2012-IEF-331795). The work at IMDEA was supported by the Campus of International Excellence (CEI) UAM+CSIC. D.B. is a FNRS Research Director. F.C. is a Royal Society Wolfson Research Merit Award holder.

## REFERENCES

- (1) Guldi, D. M.; Martin, N., Photovoltaic Applications. In *Fullerenes: From Synthesis to Optoelectronic Properties*; Springer: New York, 2002; 4, 387–435.
- (2) Hummelen, J. C.; Knight, B. W.; Lepeq, F.; Wudl, F.; Yao, J.; Wilkins, C. L. Preparation and Characterization of Fulleroid and Methanofullerene Derivatives. *J. Org. Chem.* **1995**, *60*, 532–538.
- (3) Loi, M. A.; Toffanin, S.; Muccini, M.; Forster, M.; Scherf, U.; Scharber, M. Charge Transfer Excitons in Bulk Heterojunctions of a Polyfluorene Copolymer and a Fullerene Derivative. *Adv. Funct. Mater.* **2007**, *17*, 2111–2116.
- (4) Cook, S.; Ohkita, H.; Kim, Y.; Benson-Smith, J. J.; Bradley, D. D. C.; Durrant, J. R. A Photophysical Study of PCBM Thin Films. *Chem. Phys. Lett.* **2007**, *445*, 276–280.
- (5) Kandada, A. R. S.; Grancini, G.; Petrozza, A.; Perissinotto, S.; Fazzi, D.; Raavi, S. S. K.; Lanzani, G. Ultrafast Energy Transfer in Ultrathin Organic Donor/Acceptor Blend. *Sci. Rep.* **2013**, *3*.
- (6) Noriega, R.; Rivnay, J.; Vandewal, K.; Koch, F. P. V.; Stingelin, N.; Smith, P.; Toney, M. F.; Salleo, A. A General Relationship between Disorder, Aggregation and Charge Transport in Conjugated Polymers. *Nat. Mater.* **2013**, *12*, 1038–1044.
- (7) Kim, Y.; Nelson, J.; Zhang, T.; Cook, S.; Durrant, J. R.; Kim, H.; Park, J.; Shin, M.; Nam, S.; Heeney, M.; et al. Distorted Asymmetric Cubic Nanostructure of Soluble Fullerene Crystals in Efficient Polymer:Fullerene Solar Cells. *ACS Nano* **2009**, *3*, 2557–2562.
- (8) Gelinas, S.; Rao, A.; Kumar, A.; Smith, S. L.; Chin, A. W.; Clark, J.; van der Poll, T. S.; Bazan, G. C.; Friend, R. H. Ultrafast Long-Range Charge Separation in Organic Semiconductor Photovoltaic Diodes. *Science* **2014**, *343*, 512–516.
- (9) Smith, S. L.; Chin, A. W. Ultrafast Charge Separation and Nongeminate Electron-Hole Recombination in Organic Photovoltaics. *Phys. Chem. Chem. Phys.* **2014**, *16*, 20305–20309.
- (10) Yang, Y.; Liu, C.; Gao, S.; Li, Y.; Wang, X.; Wang, Y.; Minari, T.; Xu, Y.; Wang, P.; Zhao, Y.; et al. Large 6,6-Phenyl-C-61 Butyric Acid Methyl (PCBM) Hexagonal Crystals Grown by Solvent-Vapor Annealing. *Mater. Chem. Phys.* **2014**, *145*, 327–333.
- (11) Paternó, G.; Warren, A. J.; Spencer, J.; Evans, G.; Sakai, V. G.; Blumberger, J.; Cacialli, F. Micro-Focused X-Ray Diffraction Characterization of High-Quality 6,6-Phenyl-C-61-Butyric Acid Methyl Ester Single Crystals without Solvent Impurities. *J. Mater. Chem. C* **2013**, *1*, 5619–5623.
- (12) Casalegno, M.; Zanardi, S.; Frigerio, F.; Po, R.; Carbonera, C.; Marra, G.; Nicolini, T.; Raos, G.; Meille, S. V. Solvent-Free Phenyl-C61-Butyric Acid Methyl Ester (PCBM) from Clathrates: Insights for Organic Photovoltaics from Crystal Structures and Molecular Dynamics. *Chem. Commun.* **2013**, *49*, 4525–4527.
- (13) Clulow, A. J.; Armin, A.; Lee, K. H.; Pandey, A. K.; Tao, C.; Velusamy, M.; James, M.; Nelson, A.; Burn, P. L.; Gentle, I. R.; et al. Determination of Fullerene Scattering Length Density: A Critical Parameter for Understanding the Fullerene Distribution in Bulk Heterojunction Organic Photovoltaic Devices. *Langmuir* **2014**, *30*, 1410–1415.
- (14) Savoie, B. M.; Rao, A.; Bakulin, A. A.; Gelinas, S.; Movaghar, B.; Friend, R. H.; Marks, T. J.; Ratner, M. A. Unequal Partnership: Asymmetric Roles of Polymeric Donor and Fullerene Acceptor in Generating Free Charge. *J. Am. Chem. Soc.* **2014**, *136*, 2876–2884.
- (15) Latini, G.; Downes, A.; Fenwick, O.; Ambrosio, A.; Allegrini, M.; Daniel, C.; Silva, C.; Gucciardi, P. G.; Patanè, S.; Daik, R.; et al. Optical Probing of Sample Heating in Scanning Near-Field Experiments with Apertured Probes. *Appl. Phys. Lett.* **2005**, *86*, 011102.
- (16) Dzwilewski, A.; Wagberg, T.; Edman, L. Photo-Induced and Resist-Free Imprint Patterning of Fullerene Materials for Use in Functional Electronics. *J. Am. Chem. Soc.* **2009**, *131*, 4006–4011.
- (17) Falke, S.; Eravuchira, P.; Materny, A.; Lienau, C. Raman Spectroscopic Identification of Fullerene Inclusions in Polymer/Fullerene Blends. *J. Raman Spectrosc.* **2011**, *42*, 1897–1900.
- (18) Vandenhevel, D. J.; Vandenberg, G. J. B.; Groenen, E. J. J.; Schmidt, J.; Holleman, I.; Meijer, G. Lowest Excited Singlet-State of C-

60—A Vibronic Analysis of the Fluorescence. *J. Phys. Chem.* **1995**, *99*, 11644–11649.

(19) Guss, W.; Feldmann, J.; Gobel, E. O.; Taliani, C.; Mohn, H.; Muller, W.; Haussler, P.; Termeer, H. U. Fluorescence from X-Traps in C60 Single-Crystals. *Phys. Rev. Lett.* **1994**, *72*, 2644–2647.

(20) Orlandi, G.; Negri, F. Electronic States and Transitions in C-60 and C-70 Fullerenes. *Photochem. Photobiol. Sci.* **2002**, *1*, 289–308.

(21) Sassara, A.; Zerza, G.; Chergui, M.; Negri, F.; Orlandi, G. The Visible Emission and Absorption Spectrum of C-60. *J. Chem. Phys.* **1997**, *107*, 8731–8741.

(22) Popov, A. A.; Senyavin, V. M.; Korepanov, V. I.; Goldt, I. V.; Lebedev, A. M.; Stankevich, V. G.; Menshikov, K. A.; Svechnikov, N. Y.; Boltalina, O. V.; Kareev, I. E.; et al. Vibrational, Electronic, and Vibronic Excitations of Polar C60F18 Molecules: Experimental and Theoretical Study. *Phys. Rev. B* **2009**, *79*, 045413.

(23) Zhang, Z.; Han, P.; Liu, X.; Zhao, J.; Jia, H.; Zeng, F.; Xu, B. First Principle Calculations of the Electronic Properties of the Fullerene Derivative as an Electron Acceptor in Organic Solar Cells. *J. Phys. Chem. C* **2008**, *112*, 19158–19161.

(24) Wang, H.; He, Y.; Li, Y.; Su, H. Photophysical and Electronic Properties of Five PCBM-Like C-60 Derivatives: Spectral and Quantum Chemical View. *J. Phys. Chem. A* **2012**, *116*, 255–262.

(25) Vandenhevel, D. J.; Chan, I. Y.; Groenen, E. J. J.; Matsushita, M.; Schmidt, J.; Meijer, G. On the Fluorescence of Crystalline C-60 at 1.2 K. *Chem. Phys. Lett.* **1995**, *233*, 284–290.